Submitted to
Review Scientific Instruments

A low-energy linear oxygen plasma source

André Anders[a,*] and Georgy Yu. Yushkov[b]

[a] Lawrence Berkeley National Laboratory, University of California,
1 Cyclotron Road, Berkeley, California 94720

[b] High Current Electronics Institute, Russian Academy of Sciences,
4 Academichesky Ave., Tomsk 634055, Russia

Abstract

A new version of a Constricted Plasma Source is described, characterized by all metal-ceramic construction, a linear slit exit of 180 mm length, and cw-operation (typically 50 kHz) at an average power of 1.5 kW. The plasma source is here operated with oxygen gas, producing streaming plasma that contains mainly positive molecular and atomic ions, and to a much lesser degree, negative ions. The maximum total ion current obtained was about 0.5 A. The fraction of atomic ions reached more than 10% of all ions when the flow rate was less then 10 sccm O_2, corresponding to a chamber pressure of about 0.5 Pa for the selected pumping speed. The energy distribution functions of the different ion species were measured with a combined mass spectrometer and energy analyzer. The time-averaged distribution functions were broad and ranged from about 30eV to 90 eV at 200 kHz and higher frequencies, while they were only several eV broad at 50 kHz and lower frequencies, with the maximum located at about 40 eV for the grounded anode case. This maximum was shifted down to about 7 eV when the anode was

[*] Author to whom correspondence should be addressed: Tel. +510-559-8652, Fax +510-486-4374, e-mail aanders@lbl.gov

floating, indicating the important role of the plasma potential for the ion energy for a given substrate potential. The source could be scaled to greater length and may be useful for functionalization of surfaces and plasma-assisted deposition of compound films.

Keywords: Constricted Plasma Source, oxygen plasma, ion energy distribution functions, atomic and molecular ions

I. INTRODUCTION

Oxygen plasma sources are widely used, for example for sterilization, or for the preparation of surfaces prior to deposition. The effects are manifold and include plasma-chemical etching of hydrocarbons. In the case of polymer substrates, such as webs, oxygen treatment leads to the formation of dangling bonds and the appearance of radial groups, a process known as functionalization. Cleaning and functionalization are critical for achieving superior adhesion of coatings. Oxygen plasma sources are used in assisting oxide film formation by providing "activated" oxygen in the form of ions (mainly O_2^+, O^+, and to a lesser extend also negative ions) and atoms (as opposed to O_2 molecules). Another important application is in the formation of dielectric layers in the semiconductor industry.

In many cases, oxygen plasma is provided by a filamentless source because hot filaments have a very short lifetime in the oxidizing environment. The most common sources are end-hall and closed-drift anode-layer sources,[1-3] which are capable of delivering large currents of oxygen ions at moderate energies (typically some 100 eV). This level of energy is too high for certain applications because it could lead to excessive heat load on the substrate (like polymers), or to ion damage of crystalline materials, when the ion energy is greater than the displacement energy (the latter is typically 25-35 eV)[4]. These sources are not acceptable in applications where oxide stoichiometry needs to be controlled without ion damage and physical sputtering.

At very low energy, which can be defined as energy lower than the surface and bulk displacement energies, sources of drifting *plasma* rather than ion sources are considered. In this

category, various radio-frequency (RF) and microwave plasma sources are popular.[5] However, most of these sources have a rather significant high-energy tail in the energy distribution function.

In this contribution, we introduce a new generation of the Constricted Plasma Source (CPS), a rugged, low-cost source that was previously described operating with a DC (direct current) discharge at lower power.[6-10] Some early versions of the constricted plasma source were also known as hollow anode sources.[6,7,11-13] We prefer the name constricted plasma source because it more accurately captures the physics of the discharge, which is strongly related to the formation of an electron beam formed at a double layer at a physical constriction between anode and cathode,[8,14] rather than a hollow shape of the anode. We will describe the construction of the source, provide some basic plasma diagnostics of the particles in the substrate region, and discuss the overall operational principle.

II. SOURCE CONSTRUCTION AND ELECTRICAL CONSIDERATIONS

In contrast to previous versions of the constricted plasma source,[7-9] the constriction is now a long slit and the power is one order of magnitude higher.

The new generation of the source consists essentially of a hollow cathode, an insulating spacer to a physical constriction, which in our case is a floating sheet of metal with a 180 mm long slit, and an anode, consisting of copper tubes running along the constriction. The source is made from metal and ceramic only such that it is UHV (ultra high vacuum) compatible. All metal parts are water cooled in an isolated manner. The hollow cathode was made from aluminum, with a rectangular, elongated cross section. For our tests, the slit run vertical (as one would use it in an in-line vertical sputtering system); the dimensions of the cavity were 197 mm height x 54 mm depth x 38 mm width. The constriction was made from aluminum sheet metal in which a 1-mm-wide 180-mm-long slit was machined. The choice of the constriction material is not critical: in some preliminary experiments, the constrictions were made from ceramic and stainless steel.

A manifold in the upstream region of the hollow cathode distributed the gas uniformly along the length of the source. Oxygen was selected here due to its technological importance,

but the source can operate with other gases, too. The gas flow rate was regulated by a mass flow controller (max. 200 sccm). One needs to distinguish different pressure regions: due to the constriction, the pressure in the hollow cathode cavity was obviously much higher than in the processing chamber. The chamber pressure was determined by the flow rate and pumping speed, the latter resulted from the high vacuum pump (1600 l/s for air) and an adjustable throttle valve (8" VAT valve). The base pressure of the system was about 10^{-4} Pa, and the operational pressure was between 0.1 and 1 Pa, depending on flow and selected pumping speed.

Sources of this type are generally operated continuously using regulated DC power supplies. In our case, however, using oxygen, the gas will react with the electrode components and form an oxide, which could readily lead to arcing on the cathode surface. This situation is well known in the field of reactive sputter deposition, where a standard solution involves medium-frequency chopping of the applied cathode (target) voltage. The idea behind pulsing is to let the cathode sheath collapse in-between pulses such that electrons from the plasma can reach the cathode surface and neutralize the positive surface charge, thereby removing the main cause for arcing. To promote this process, a brief time of reverse polarity is applied after each negative pulse to the cathode. The same idea was applied here to the operation of the oxygen plasma source. So-called "pulsed-DC" power was provided from a 5 kW Pinnacle® Plus power supply (Advanced Energy), with frequencies up to 350 kHz. As we observed, the arcing probability decreased dramatically when the frequencies was set to 50 kHz or higher. When an arc occurred, the power supply's fast arc suppression feature briefly interrupted the power flow before restoring normal operation.

In this report, we investigated the range of frequencies from 5 kHz (period 200 μs) to 350 kHz (period 2.86 μs) with reversal times in the range of 5 μs and 700 ns, respectively. Due to arcing at low frequencies, the reported data were taken for 50 kHz and greater. The power was limited to a maximum of 1500 W to avoid possible damage to the source; the actual power limit of the source is unknown. Fig. 1 shows a typical current and voltage trace for the source in operation. The current in the reversal time was high (the hollow cathode set to positive potential) because electrons have a high mobility.

III. SETUP OF CHARACTERIZATION EXPERIMENTS

Most of the plasma diagnostics was done using a plasma analyzer (EQP by Hiden Ltd) capable of determining particle species via its quadrupole mass spectrometer, and their energy distribution functions via its electrostatic energy filter. The analyzer had a grounded entrance tube with an orifice of 100 μm diameter. The device was differentially pumped and can be used in the whole pressure range of interest. The distance between plasma source and plasma analyzer can be varied but was 20 cm for most of the measurements (Fig. 2).

Alternatively to the plasma analyzer, a very large area (700 cm^2), biased ion collector was placed in front of the EPQ entrance. The bias voltage for ion collection was set to 120 V negative to ground, thereby ensuring that ion saturation was achieved while secondary electron emission was still negligible. This device allowed us to determine the total ion current available. The particle measurements were complemented by basic plasma optical emission spectrometry using a Telemark TCM 420 spectrometer (max resolution 0.35 nm on a cooled CCD detector array, 1024 x 256 pixels, 16 bit digital resolution). Light was collected in side-on geometry, relative to the plasma flow, from an area near the slit to about 5 cm downstream of the slit. The light was imaged onto an optical quartz fiber and guided to the entrance slit of the spectrometer. Spectral line identification was done using the device library (software) and standard spectral tables.

IV. RESULTS

By varying gas flow and power settings, it was quickly evident that the source can operate in a wide range of parameters. As expected, the plasma production was concentrated at the constriction. An initial survey of species, using the plasma analyzer, revealed the presence of molecular and atomic neutrals and ions. Their time-averaged energy distribution functions for the different particles looked similar and always depended on the frequency settings of the power supply (Fig. 3). At high frequencies, the distributions were very broad; they became much narrower at low frequencies (50 kHz). This was true for both ionized and neutral species, indicating the important role of energy exchange by collisions, especially by charge exchange collisions.

The narrower distributions and thus better-defined particle energies suggested operating at low frequencies, however, low frequencies led to enhanced arcing probability. Therefore, 50

kHz was determined to be an optimized frequency, which was used in most experiments because both factors were satisfactorily taken into account.

For many applications it is desirable to have a high fraction of atomic ions and radicals because these species most readily react on the substrate surface with vapor, thereby forming a compound film. We focus here on the ion components of the plasma because they can be directly measured without using the RF ionization stage after the analyzer's entrance aperture. Results for atomic and molecular positive ions are shown in Figs. 4 and 5. A maximum $O^+/(O_2^+ + O^+)$ ratio of more then 10% was observed for low flow and low pressure conditions, when the discharge voltage was high. The same data are plotted again in Fig. 6, though this time as a function of the discharge voltage. One can see a non-linear behavior for the ion energies but a nearly linear behavior for the ion fluxes.

The measured ion energies were somewhat higher than anticipated (based on measurements for low-power nitrogen operation[8]), which was attributed to the plasma potential of the new system investigated. It is known that the plasma potential can be directly influenced by selecting the anode potential. Therefore, in order to find a practicable approach to obtaining the desired low energies, the anode was removed from ground and the discharge system became floating, i.e., the plasma potential was self-establishing by interaction with the grounded chamber. Removing the ground caused indeed a significant shift in the ion energy of both molecular and atomic ions (Fig. 7). One can notice that the energy distribution functions are not just shifted but they have broadened and changed amplitude. Therefore, it seemed necessary to repeat all of the previous measurements of atomic and molecular ion fluxes and discharge voltage but this time with a floating anode. The results are presented in Figs. 8-10. The fraction of atomic ions reached more than 10%, which was not significantly different than what was found with a grounded anode.

While the EQP analyzer is well suited to measure the relative fluxes of ion species, a negatively biased ion collector was needed to determine the total ion flux and thereby calibrate the fluxes of the individual species. Fig. 11 shows the total ion fluxes for the grounded and floating anode cases. The maximum ion current was about 0.5 A for the power of 1.5 kW at a flow of 25 sccm and a corresponding pressure of about 0.8 Pa.

The probe measurements were supplemented by some basic optical emission spectroscopy (OES). There is a general trend to emission with shorter wavelength as the pressure is decreased (Fig. 12), indicating more energetic excitation conditions (higher electron temperature, higher degree of dissociation and ionization). The spectrum contains emission lines of atomic species (O, O^+) as well as molecules (O_2, O_2^+). The spectrum at higher pressure is dominated by the broadband emission of ionic molecular oxygen at 642, 616, 686, 563, and 524 nm due to transitions from $^4\Sigma_g^-$ to $^4\Pi_u$; one can also clearly see the excited atomic oxygen lines at 844 and 777 nm due to electron transitions from $3p\ ^3P$ to $3s\ ^3S$ and from $3p\ ^5P$ to $3s\ ^5S$, respectively. The apparent absence of these lines at the lowest pressure, 0.13 Pa, does not mean absence of these atoms but rather drastically shifted excitation conditions. A detailed analysis is rather involved and beyond the scope of this report.

III. SOURCE OPERATIONAL PRINCIPLE AND DISCUSSION OF RESULTS

Oxygen gas is introduced into the hollow cathode cavity and a high negative potential is applied to the cathode with respect to the anode. The anode is the reference potential that is commonly grounded, however, it can be removed from ground in order to control the ion energy distribution. The initial voltage from the Pinnacle power supply can be as high as 1700 V to facilitate the ignition of the discharge, which occurs readily provided the gas pressure inside the source is sufficiently high, typically about 10 Pa.

The cavity shape of the cathode ensures the hollow cathode effect, i.e., a repeated reflection of electrons by opposing sheaths. The electrons cross the cavity until a collision occurs. Therefore, the mean free path for ionizing collisions can be much larger than the cavity dimension and yet intense ionization can occur at relatively low pressure. Ions arriving at the cathode surface contribute to current transport and generate secondary electrons which become "hot" electrons by crossing the cathode sheath (their energy is determined by the cathode fall, which is typically 400 V or greater).

In principle, the constricted plasma source can be operated with a planar cathode, i.e., without the hollow cathode effect. However, using a hollow cathode gives the source greater discharge current capability, which promotes the constriction effect and results in greater source

output. The constriction effect is related to the formation of an electrical double layer at the constriction.[6]

We will estimate the constriction effect using the source geometry with hollow cathode. Following considerations by Metel,[15] the mean path length before an electron is lost to the hollow cathode opening (i.e. the effective anode, or virtual anode in our slit constriction geometry), can be estimated by

$$\lambda_{loss} \approx 4V_{HC} / A_{slit} , \tag{1}$$

where V_{HC} is the volume of the hollow cathode and A_{slit} is the slit area. In our case, $V_{HC} \approx 4\times10^5$ mm^3, $A_{slit} = 180$ mm^2 and therefore $\lambda_{loss} \approx 9$ m. The pressure inside the cavity should be high enough to allow the energetic electron to make a collision before being lost. Indeed, the ionization and thermalization lengths, λ_e and λ_{therm}, are much smaller than the geometric loss length,[16]

$$\lambda_e = \left(P_i\ p_{HC}\right)^{-1} \ll \lambda_{therm} = \frac{eV_c}{E_i}\lambda_e \ll \lambda_{loss} , \tag{2}$$

where P_i is the ionization probability, p_{HC} is the pressure in the hollow cathode, V_c is the cathode fall voltage, and E_i is the energy transferred in an ionization collision. For an estimate, one may use $V_c = 400$ V, $E_i \approx 20$ eV, $P_i \approx 10$ Pa^{-1} m^{-1}, $p_{HC} \approx 10$ Pa, hence $\lambda_e \approx 0.01$ m and $\lambda_{therm} \approx 0.2$ m, i.e., most of the originally hot electrons have lost their energy when they happen to be near the slit region.

A virtual anode forms at the slit such as to facilitate transport of the thermal electrons to the anode, which is necessary to close the electrical current circuit. The virtual anode is a curved double layer in which electrons are accelerated, enabling them to pass the constriction and do more inelastic collisions. The intense plasma near a circular constriction is sometimes described as a "plasma ball"[17].

A criterion for the formation of a double layer can be formulated by comparing the currents to the surface of the hollow cathode and to the constriction. Kirchhoff's law (current continuity) can be written as[18]

$$0.4(1+\gamma)\,e\,n\,A_{HC}\sqrt{\frac{2kT_e}{M_i}} = e\,n\,A_{slit}\sqrt{\frac{kT_e}{2\pi m_e}} \tag{3}$$

where A_{HC} is the area of the hollow cathode, γ is the secondary electron yield, k is the Boltzmann constant, T_e is the electron temperature, and M_i and m_e are the ion and electron mass, respectively. Using $\gamma \approx 0.1$ [19], one finds

$$\frac{A_{slit}}{A_{HC}} \le 1.6\sqrt{\frac{m_e}{M_i}} = 6\times10^{-3} \tag{4}$$

as a criterion for the onset of virtual anode formation. That is, if the slit area is smaller than the critical value described by (4), a curved double layer appears that assists electron transport. The cavity-facing surface of the double layer represents a virtual anode that bulges into the hollow cathode; it is curved such as to have a greater area than the constriction, hence electron collection and guiding through the slit are facilitated. In our case, A_{slit}/A_{HC} is slightly smaller than 6×10^{-3} and therefore a double layer is indeed expected.

Curvature and voltage drop can be estimated using certain boundary and shape assumptions when solving the Poisson equation for space charge limited transport. The approximation by the Child-Langmuir law is adequate for this estimate, and the area of the electron-collecting double layer can be found by assuming that Eq. (4) is marginally satisfied, i.e., $A_{DL} = 6\times10^{-3}\,A_{HC} \approx 200\ \mathrm{mm}^2$. Assuming that the boundary along the slit is semi-cylindrically curved and bulging into the plasma region of the hollow-cathode cavity, can find that the largest distance of the curved surface from the planar slit plane is about 150 μm. To transport the electron current through the slit, the Child Langmuir law gives $V_{DL} \approx 25\ \mathrm{V}$ for a discharge current of 3 A, corresponding to a current density of $j_e \approx 15\ \mathrm{mA/mm}^2$. Electrons passing through the double layer get an energetic boost of about 25 eV, enabling them to make ionizing collisions outside the plasma source. This is a key feature of the plasma source: thanks to energetic electrons formed at the constriction, relatively dense plasma is formed right at the constriction where the gas pressure is still high.

Using again the ionization probability of $P_i \approx 10\ \mathrm{Pa^{-1}\ m^{-1}}$, ref.[16], and a transitional pressure of about 1 Pa, the ionization length is 0.1 m, which is of the same order of magnitude as

the distance between the source and the anode or a wall or a substrate. This implies that the likelihood for ionization is moderate near the slit and much smaller far from the source where the pressure has dropped towards to chamber pressure. This also implies that when operating at relatively low pressure, many electrons will not ionize the gas but keep moving as an energetic beam toward the chamber wall or other component placed the electron beam path. At low pressure, the source can be considered as an *electron* ribbon source, while at higher pressures it is a source of low energy plasma, where significant plasma production occurs near the constriction slit outside the actual source. For an estimate one can use a cross section of (1-2) 10^{-15} cm^2, ref.[16], leading to a probability of charge exchange of 0.25-0.5 $cm^{-1}Pa^{-1}$, and a mean free path of 0.25-0.5 cm at 1 Pa. Hence, a charge exchange collision is probable before the ion reaches the analyzer.

After we have described the basic processes of the plasma source, we will now turn to the discussion of the measured data. The rather dramatic change of the time-averaged energy distribution functions as the discharge frequency is reduced, Fig. 3, is clearly related to the transient processes of the plasma. Specifically, one should expect that the plasma potential is not constant but subject to periodic shifts, which in turn will cause the sheath in front of the energy analyzers to pulsate. At high frequency, the relative duration of more positive plasma potential is enhanced, leading to significantly enhanced ion energies with respected to the grounded analyzer. The non-stationary and nonlinear features are apparent from the non-monotonous character of the time-averaged distribution function. For a deeper understanding, time-resolved measurements of the potential are needed.

The non-monotonic behavior of ion energy and flux with increasing gas flow and pressure requires that counteracting processes play a role. The most obvious to consider are power input per particle, energy exchange between particles, and shifts in plasma potential. Since the power was kept constant (1.5 kW), reducing the flow (and pressure) implies that more energy is available for each particle, which can lead to higher electron temperature, and greater excitation, dissociation, and ionization. This will directly influence the ratio of atomic to molecular species, and indeed, we see more atomic species at lower pressure. When the pressure is increased, the likelihood for collisions is increased; which, on the one hand, can lead to the production of more ions and hence an increase in the total ion flux (Fig. 10). On the other hand, after reaching a maximum, this current decreases because yet higher pressure reduces the

electron temperature as well as increases the probability of charge exchange collisions, recombination, and scattering of ions such that they are not captured by the ion collector.

The non-monotonic behavior of the ion energy is clearly determined by the plasma potential, as a comparison of Figs. 6 and 10 shows. Generally, one would expect that increased discharge voltage would systematically increase the plasma potential and thus the measured ion energy, which is the case for the floating anode (Fig. 11). However, when the potential of the anode is fixed, the plasma potential is not only influenced by the absolute discharge voltage but by the balance of charge particles to the grounded components. The ion flux is known to be non-monotonic, see Fig. 11, and similarly the ion flux to grounded components is non-monotonic. The issue of particle balance is complicated by the fact that the particle fluxes are not thermal but have drift character (ions, due to pressure gradient) or even beam character (electrons, due to acceleration in the constriction's double layer).

While these qualitative arguments can be used to explain the source properties, modeling is required for quantitative understanding. The complicated boundary conditions, time dependencies, and complicated plasma chemistry involving atomic and molecular species make this task clearly beyond the scope of this report.

ACKNOWLEDGEMENTS

The authors thank Michael Dickinson for technical support. This work was supported by the Assistant Secretary for Energy Efficiency and Renewable Energy, Office of Building Technology, and the Office of Nonproliferation and International Security, Initiatives for Proliferation Prevention, Project No. IPP-LBNL-T2-196, both of the U.S. Department of Energy, under Contract No. DE-AC02-05CH11231 with the Lawrence Berkeley National Laboratory.

REFERENCES

[1] H. R. Kaufman, R. S. Robinson, and R. I. Seddon, J. Vac. Sci. Technol. A **5,** 2081 (1987).

[2] A. M. Dorodnov, S. A. Muboyadzhyan, Y. A. Pomelov, and Y. A. Strukov, Zhurnal Prikladnoi Mekhaniki i Tekhnicheskoi Fiziki **22,** 35 (1981).

[3] A. Fruchtman, N. J. Fisch, and Y. Raitses, Phys. Plasmas **8,** 1048 (2001).

[4] W. Eckstein, *Computer Simulation of Ion-Solid Interactions* (Springer-Verlag, Berlin, 1991).

[5] *High Density Plasma Sources*; *Vol.*, edited by O. A. Popov (Noyes, Park Ridge, N.J., 1995).

[6] A. Anders and S. Anders, Plasma Sources Sci. Technol. **4,** 571 (1995).

[7] A. Anders, N. Newman, M. Rubin, M. Dickinson, E. Jones, P. Phatak, and A. Gassmann, Rev. Sci. Instrum. **67,** 905 (1996).

[8] A. Anders and M. Kühn, Rev. Sci. Instrum. **69,** 1340 (1998).

[9] A. Anders, R. A. MacGill, and M. Rubin, IEEE Trans. Plasma Sci. **27,** 82 (1999).

[10] A. E. Zhukov, R. Zhao, P. Specht, V. M. Ustinov, A. Anders, and E. R. Weber, Semiconductor Sci. Technol. **16,** 413 (2001).

[11] V. I. Miljevic, Appl. Optics **23,** 1598 (1984).

[12] V. I. Miljevic, Rev. Sci. Instrum. **61,** 312 (1990).

[13] V. Miljevic, Rev. Sci. Instrum. **63,** 2619 (1992).

[14] R. H. Varey, J. Smalley, P. H. Richards, and C. F. Gozna, J. Phys. D: Appl. Phys. **4,** 1520 (1971).

[15] A. Metel, Surf. Coat. Technol. **156,** 38 (2002).

[16] Y. P. Raizer, *Gas Discharge Physics* (Springer-Verlag, Berlin, 1991).

[17] V. Miljevic, J. Appl. Phys. **60,** 4109 (1986).

[18] A. S. Metel', Sov. Phys. - Techn. Phys. **29** (1984).

[19] M. Kaminsky, *Atomic and Ionic Impact Phenomena on Metal Surfaces* (Springer-Verlag, Berlin, 1965).

Figure Captions

Fig. 1. (Color online). Current and voltage of the oxygen plasma source with the Pinnacle Plus set to 250 kHz. The current was measured inductively using a Pearson coil, 0.01 V/A (bandwidth 50 MHz), and the voltage using a Tektronix 1000:1 voltage probe (bandwidth 20 MHz).

Fig. 2. Setup of the plasma source and plasma analyzer; the insert shows a photograph of the source.

Fig. 3. (Color online). Energy distribution functions of O_2^+ ions, 1.3 Pa O_2, at a discharge power of 1.5 kW.

Fig. 4. (Color online). Total currents of atomic and molecular oxygen ions, as determined by the EQP detector count rates, and the ratio of the these ion fluxes, presented as a function of oxygen flow and resulting chamber pressure.

Fig. 5. (Color online). Most likely ion energy (peak of the distribution function), and discharge voltage, as a function of gas flow and resulting chamber pressure.

Fig. 6. (Color online). Data of figure 6 plotted as a function of the discharge voltage, indicating the qualitatively different behaviors of ion energy and ion flux.

Fig.7. (Color online). Energy distribution functions of molecular (top) and atomic (bottom) ions with grounded and floating anode (as indicated).

Fig.8. (Color online). As figure 4 but with floating anode.

Fig. 9. (Color online). As figure 6 but with floating anode.

Fig. 10 As figure 6 but with floating anode; both energy and fluxes show now approximately linear dependence on the discharge voltage.

Fig. 11. (Color online). Total ion current, time averaged, as measured by a large, negatively biased ion collector.

Fig. 12. (Color online). Optical emission spectra of oxygen plasma at a constant power of 1.5 kW for different flows and corresponding chamber pressures, as indicated.

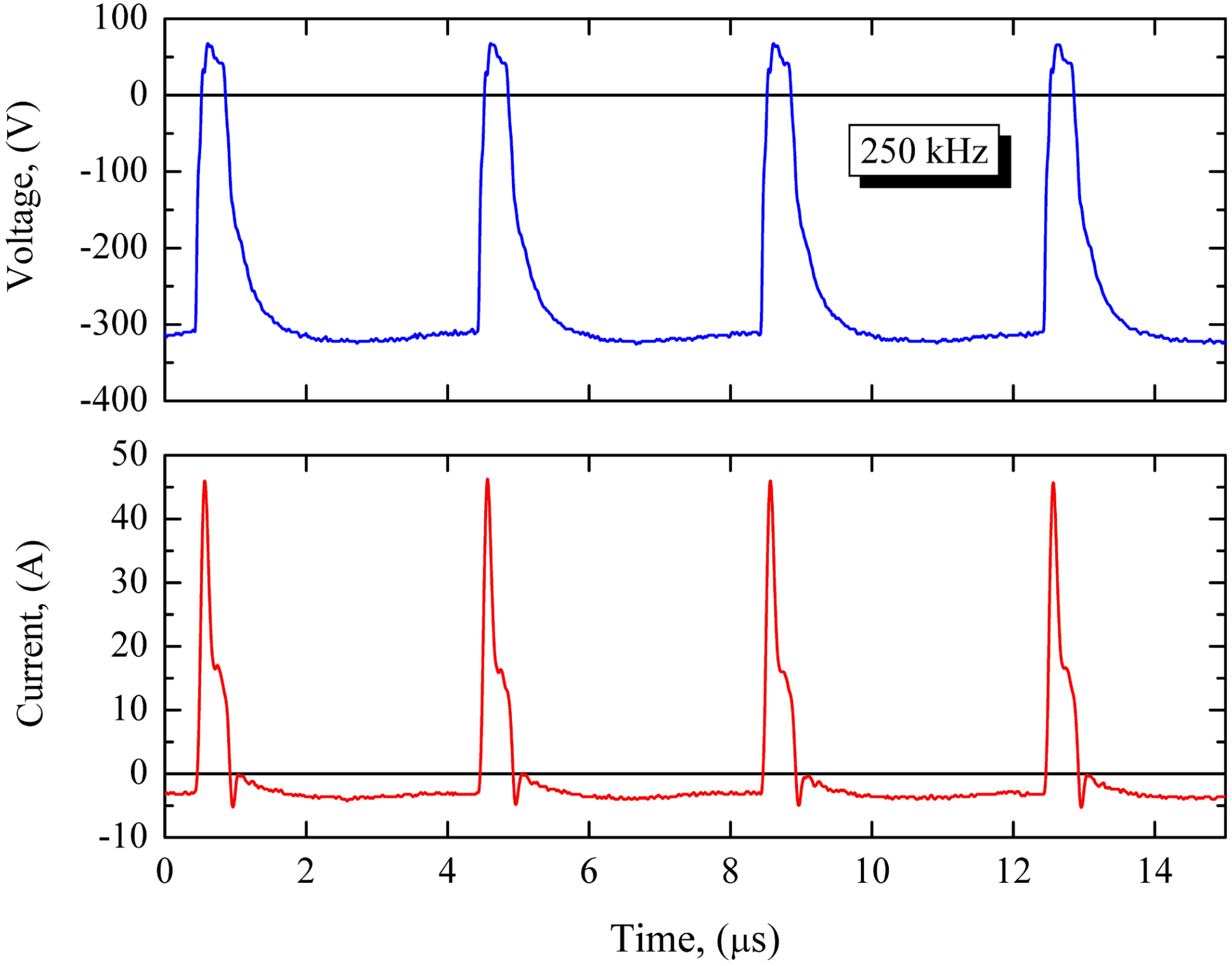
Voltage, (V)
100
0
-100
-200
-300
-400
250 kHz
Current, (A)
50
40
30
20
10
0
-10
0
2
4
6
8
10
12
14
Time, (μs)

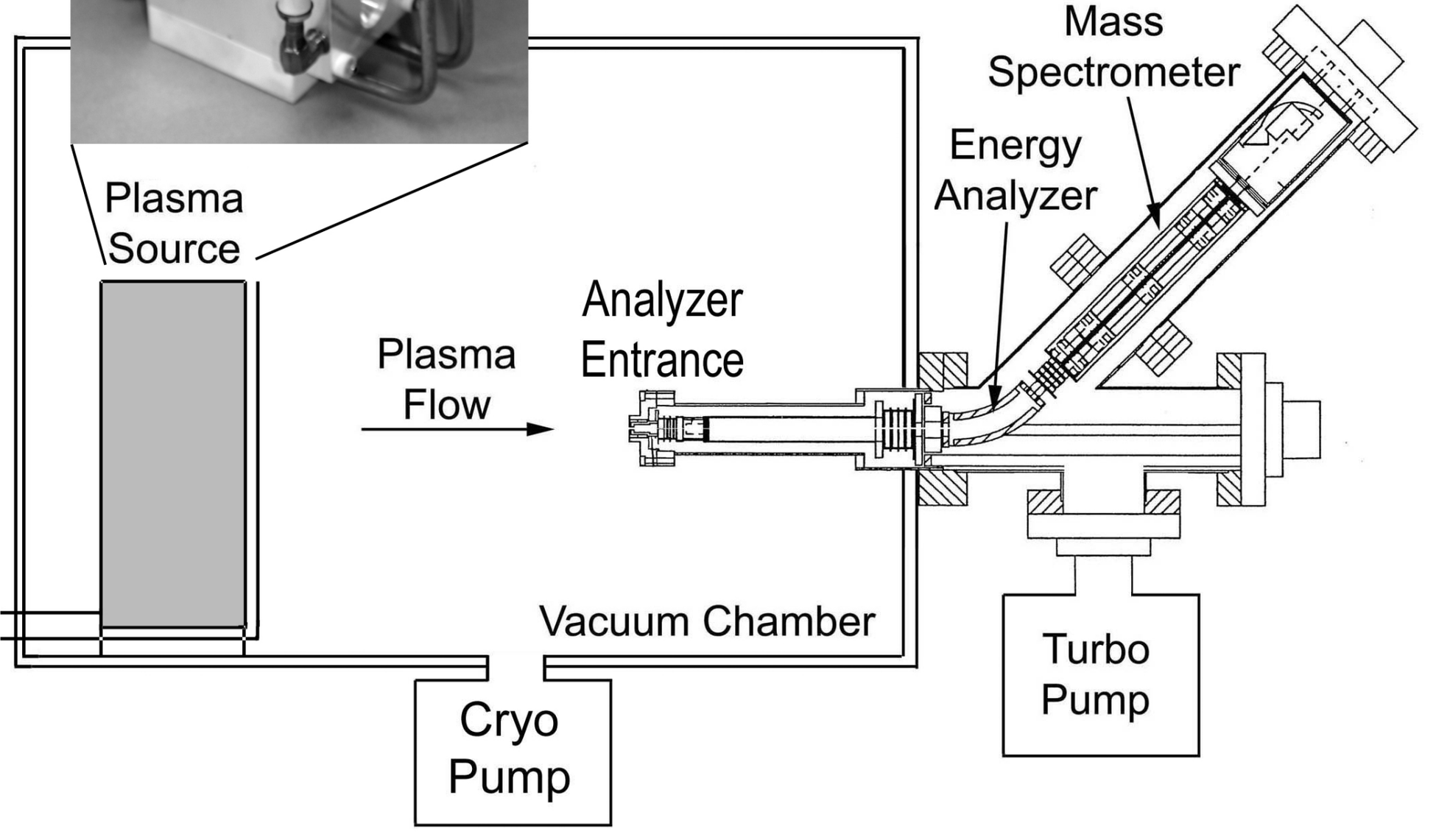
Mass
Spectrometer
Energy
Analyzer
Plasma
Source
Analyzer
Entrance
Plasma
Flow
Vacuum Chamber
Turbo
Pump
Cryo
Pump

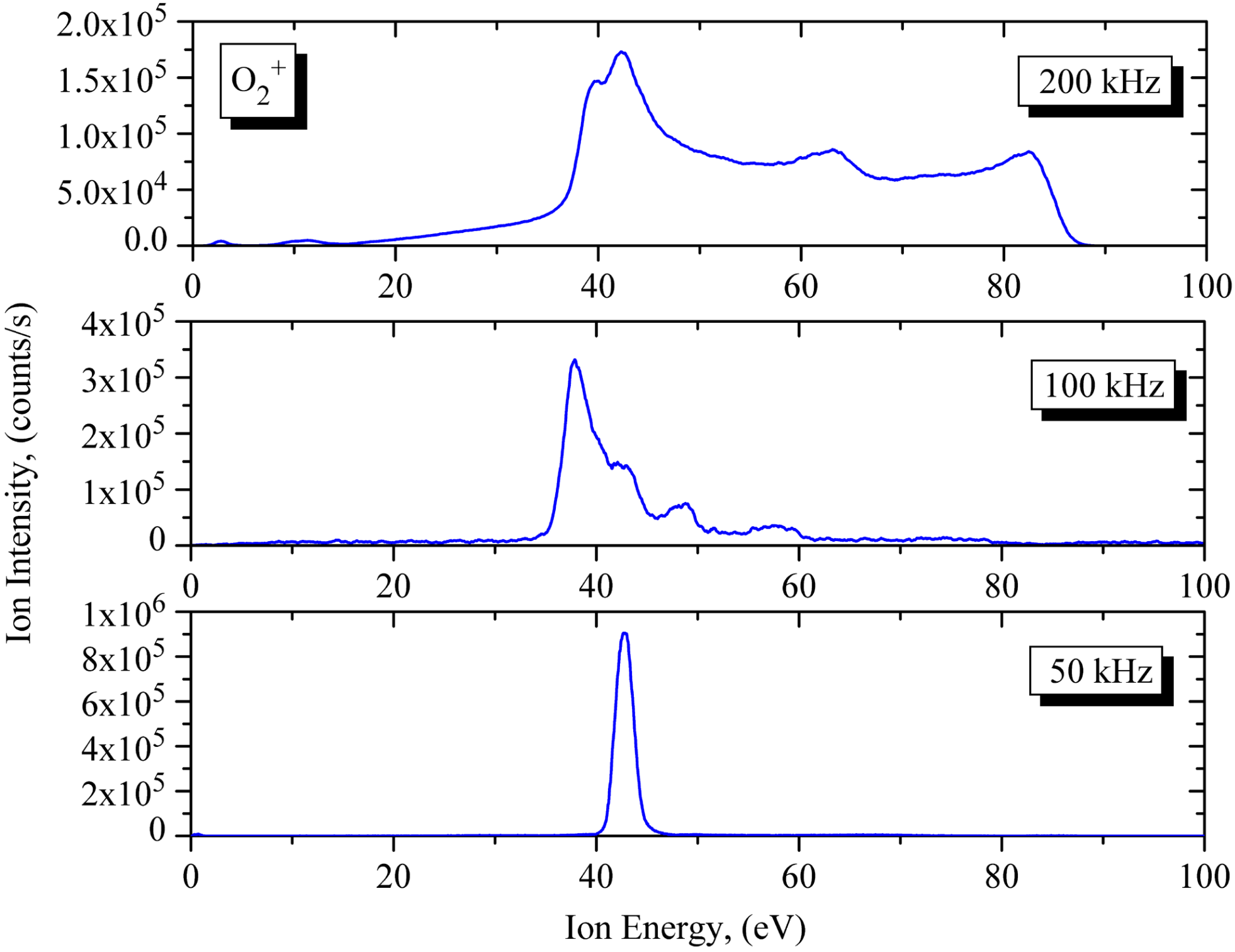
O_2^+
200 kHz
100 kHz
50 kHz
Ion Intensity, (counts/s)
Ion Energy, (eV)
2.0x10^5
1.5x10^5
1.0x10^5
5.0x10^4
0.0
4x10^5
3x10^5
2x10^5
1x10^5
0
1x10^6
8x10^5
6x10^5
4x10^5
2x10^5
0
0
20
40
60
80
100

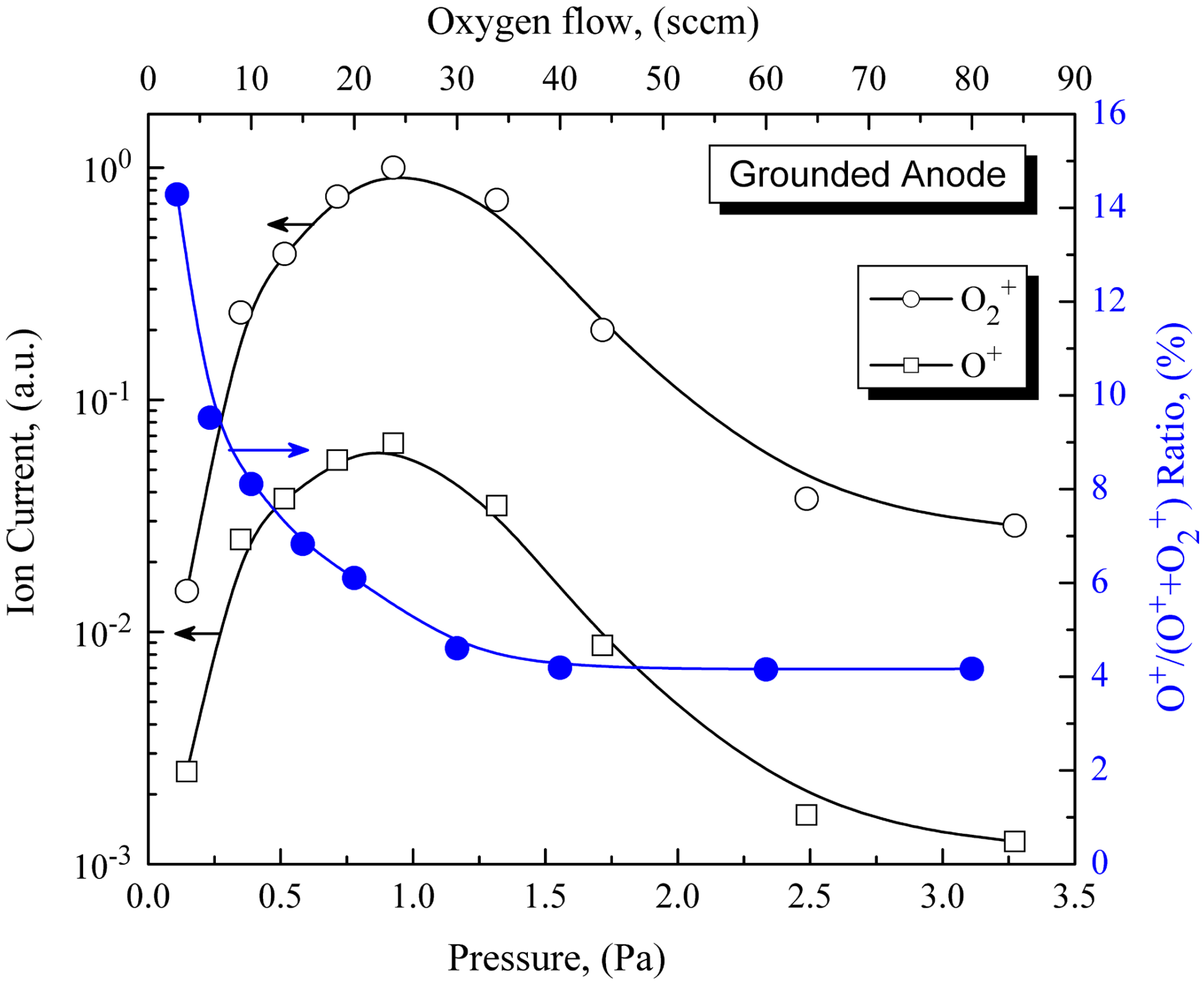
Oxygen flow, (sccm)
0
10
20
30
40
50
60
70
80
90
Grounded Anode
O_2^+
O^+
Ion Current, (a.u.)
10^0
10^{-1}
10^{-2}
10^{-3}
$O^+/(O^+ + O_2^+)$ Ratio, (%)
16
14
12
10
8
6
4
2
0
0.0
0.5
1.0
1.5
2.0
2.5
3.0
3.5
Pressure, (Pa)

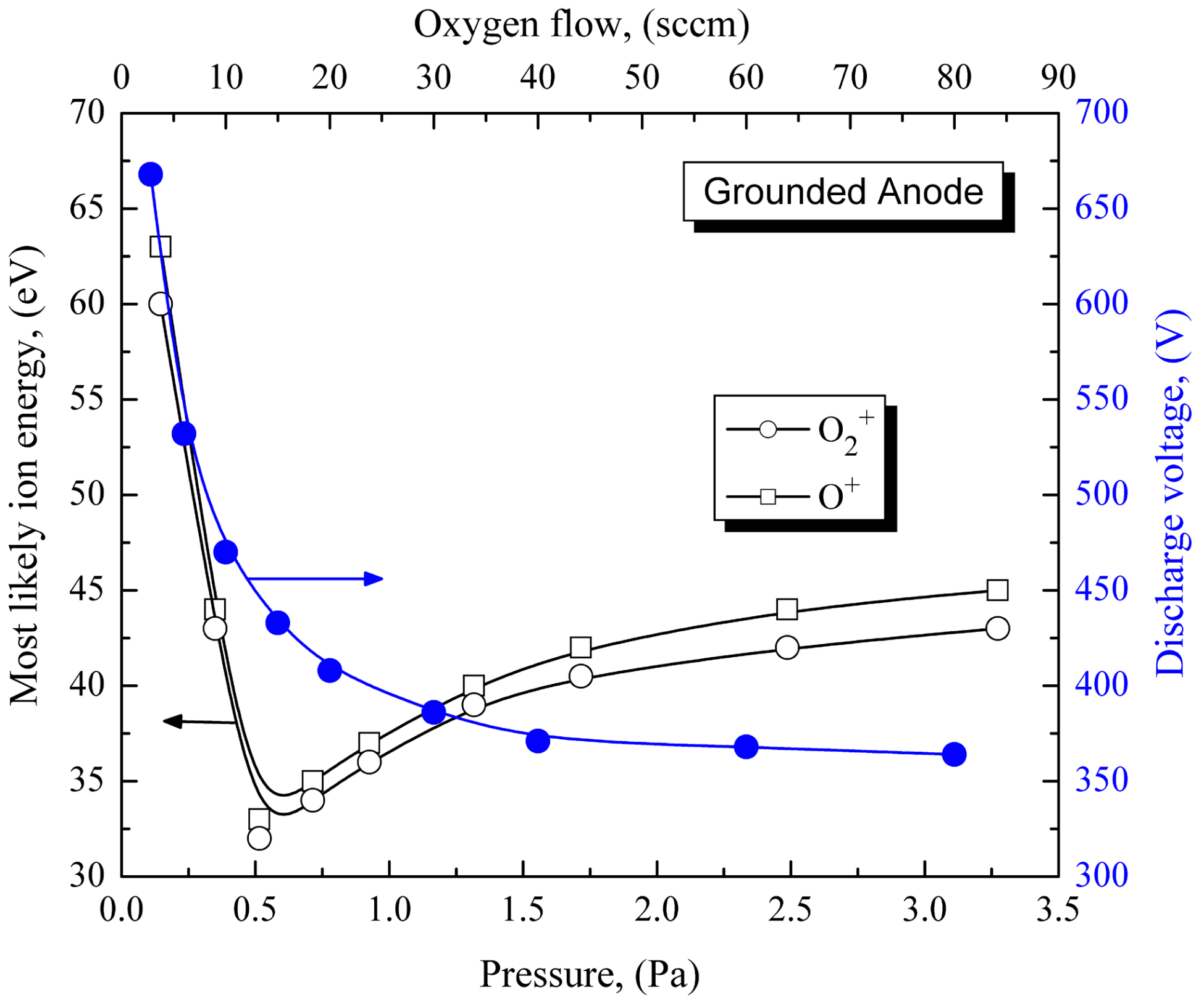
Oxygen flow, (sccm)
0
10
20
30
40
50
60
70
80
90
Grounded Anode
O_2^+
O^+
Most likely ion energy, (eV)
Discharge voltage, (V)
Pressure, (Pa)
0.0
0.5
1.0
1.5
2.0
2.5
3.0
3.5
30
35
40
45
50
55
60
65
70
300
350
400
450
500
550
600
650
700

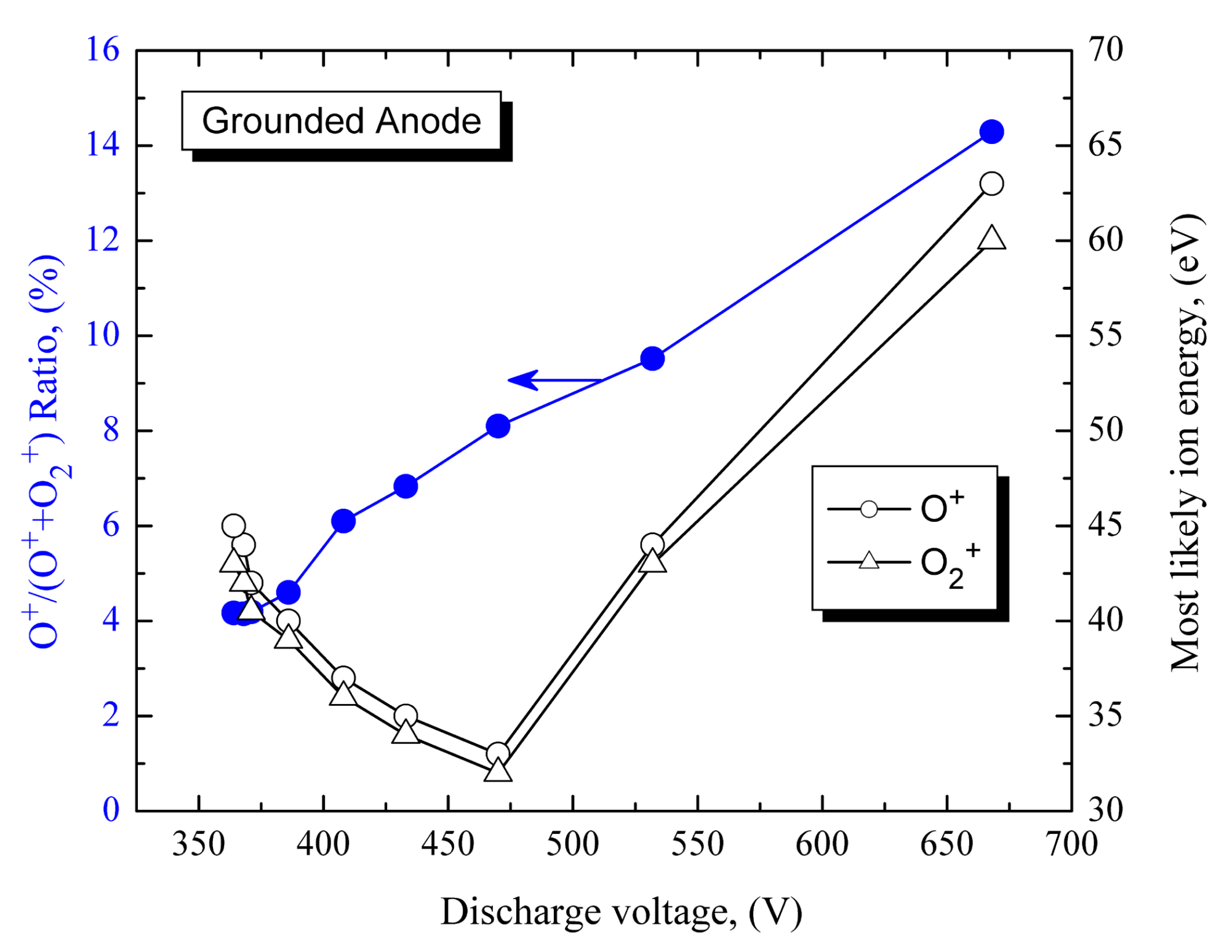
Grounded Anode
O^+
O_2^+
$O^+/(O^+ + O_2^+)$ Ratio, (%)
Most likely ion energy, (eV)
Discharge voltage, (V)
0
2
4
6
8
10
12
14
16
30
35
40
45
50
55
60
65
70
350
400
450
500
550
600
650
700

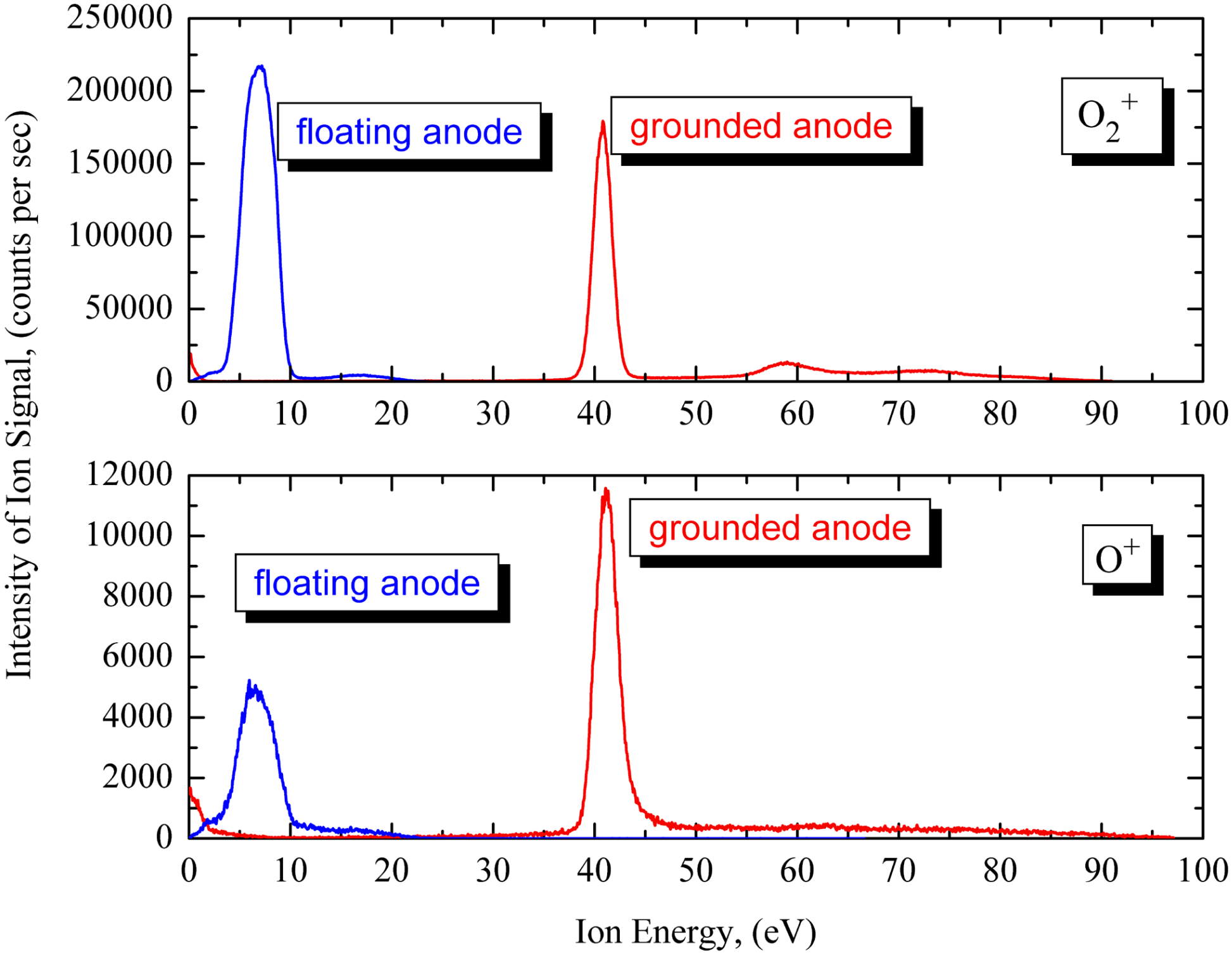
Intensity of Ion Signal, (counts per sec)
250000
200000
150000
100000
50000
0
floating anode
grounded anode
O_2^+
0
10
20
30
40
50
60
70
80
90
100
12000
10000
8000
6000
4000
2000
0
floating anode
grounded anode
O^+
0
10
20
30
40
50
60
70
80
90
100
Ion Energy, (eV)

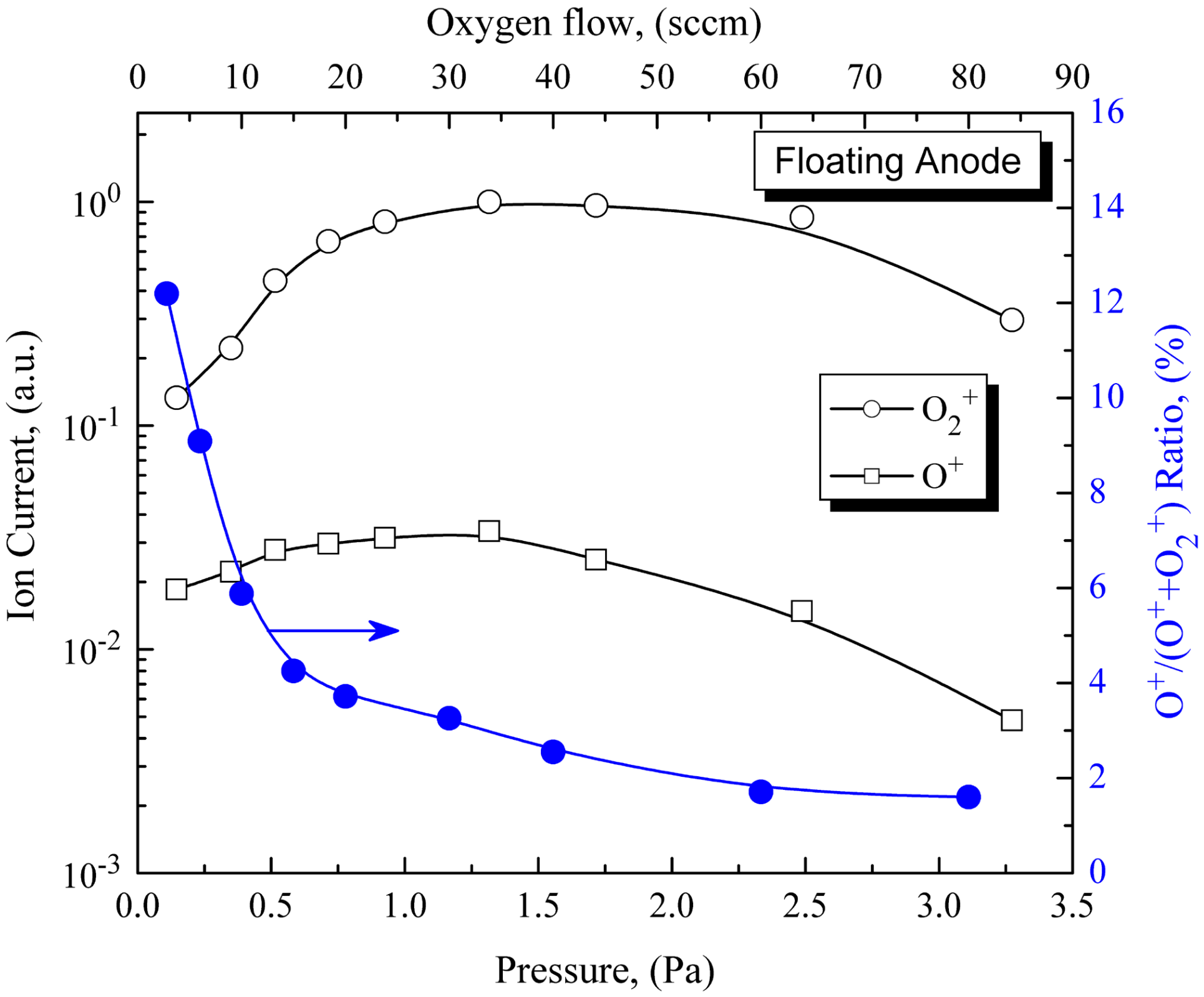
Oxygen flow, (sccm)
0
10
20
30
40
50
60
70
80
90
Floating Anode
O_2^+
O^+
Ion Current, (a.u.)
10^0
10^{-1}
10^{-2}
10^{-3}
$O^+/(O^+ + O_2^+)$ Ratio, (%)
16
14
12
10
8
6
4
2
0
0.0
0.5
1.0
1.5
2.0
2.5
3.0
3.5
Pressure, (Pa)

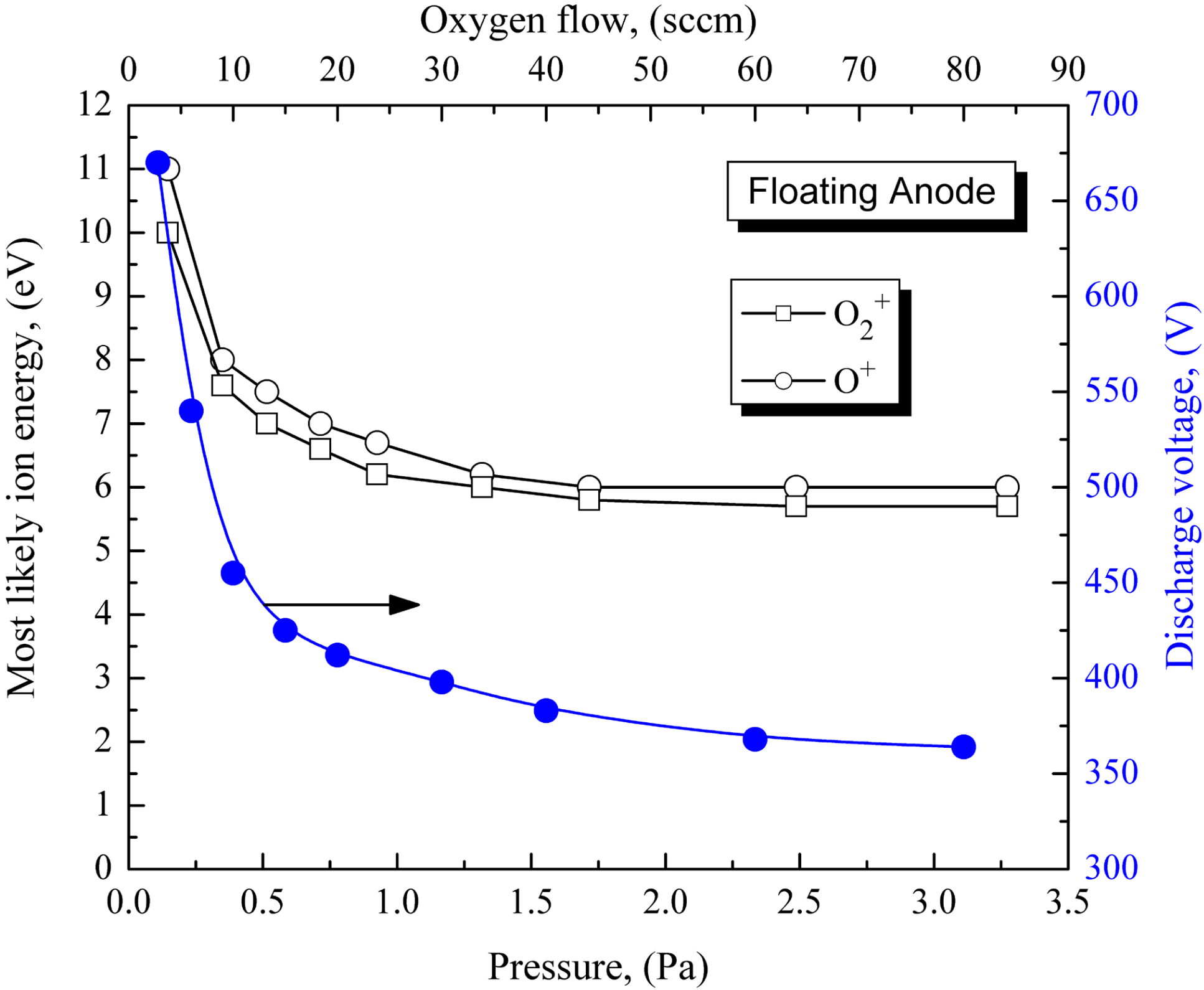
Oxygen flow, (sccm)
0
10
20
30
40
50
60
70
80
90
Most likely ion energy, (eV)
Discharge voltage, (V)
Floating Anode
O_2^+
O^+
Pressure, (Pa)
0.0
0.5
1.0
1.5
2.0
2.5
3.0
3.5

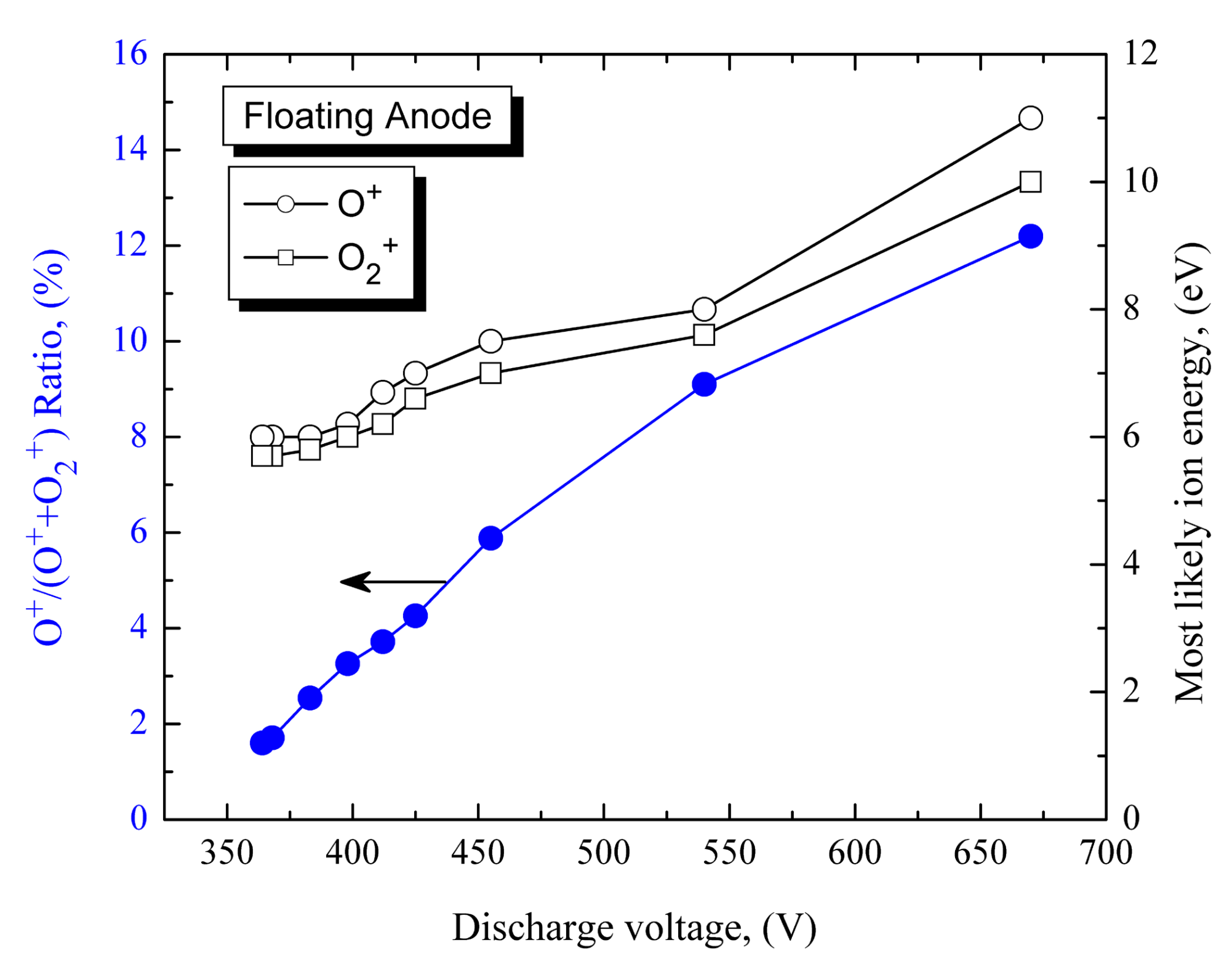
Floating Anode
O+
O2+
O+/(O++O2+) Ratio, (%)
Most likely ion energy, (eV)
Discharge voltage, (V)
0
2
4
6
8
10
12
14
16
0
2
4
6
8
10
12
350
400
450
500
550
600
650
700

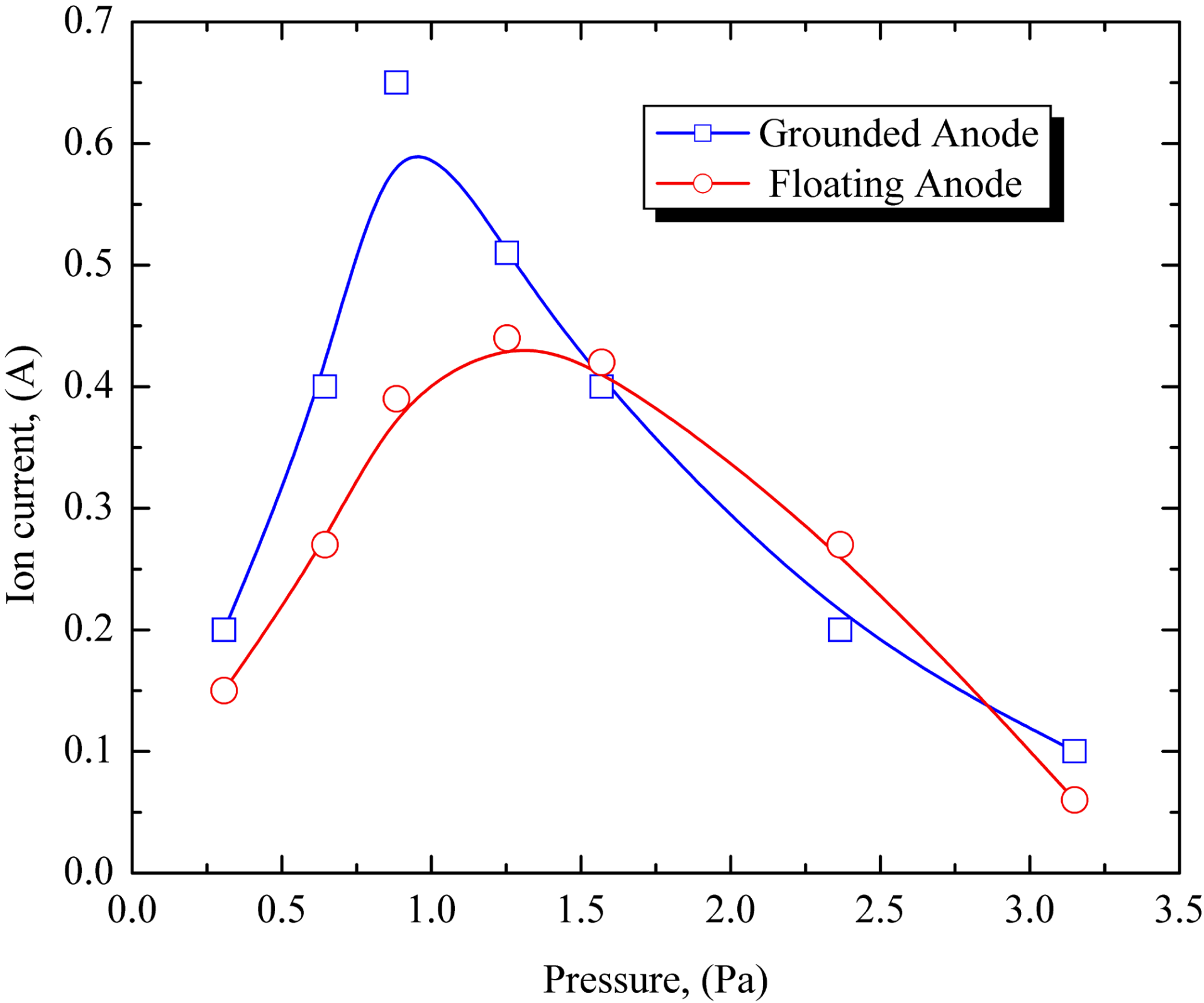
Grounded Anode
Floating Anode
Ion current, (A)
Pressure, (Pa)
0.0
0.1
0.2
0.3
0.4
0.5
0.6
0.7
0.0
0.5
1.0
1.5
2.0
2.5
3.0
3.5

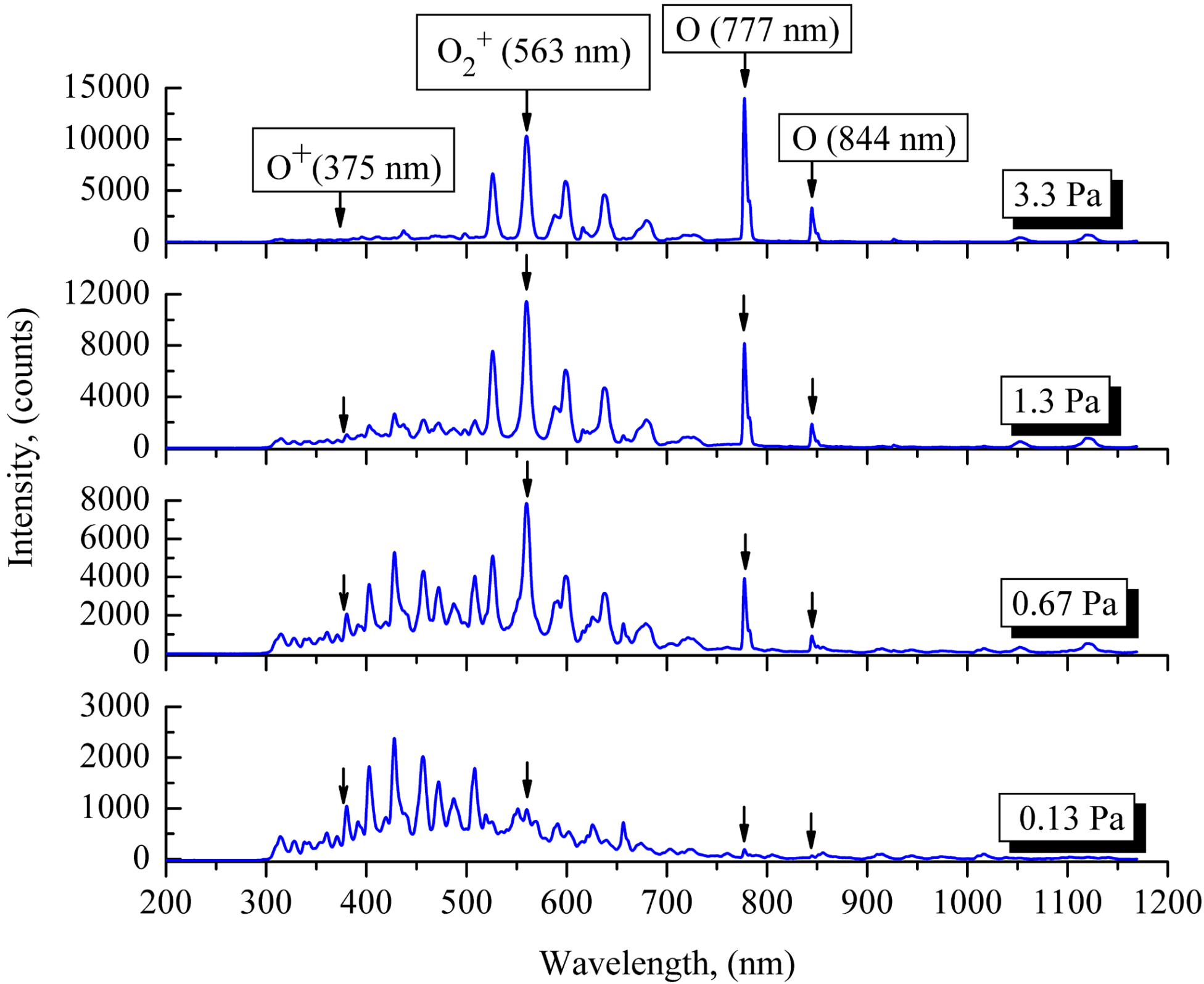
O (777 nm)
O2+ (563 nm)
O (844 nm)
O+(375 nm)
3.3 Pa
1.3 Pa
0.67 Pa
0.13 Pa
Intensity, (counts)
Wavelength, (nm)
15000
10000
5000
0
12000
8000
4000
0
8000
6000
4000
2000
0
3000
2000
1000
0
200
300
400
500
600
700
800
900
1000
1100
1200